ChemComm

COMMUNICATION

View Article Online
View Journal | View Issue

Cite this: *Chem. Commun.*, 2017, 53, 9097

Received 11th June 2017,
Accepted 24th July 2017

DOI: 10.1039/c7cc04523a

rsc.li/chemcomm

A highly conductive carbon–sulfur film with interconnected mesopores as an advanced cathode for lithium–sulfur batteries†

Mingkai Liu,[a] Yuqing Liu,[a] Yan Yan,*[a] Fengsheng Wang,[a] Jiahui Liu[a] and Tianxi Liu *[ab]

A highly conductive graphene sheet–mesoporous carbon (MC) sphere/active sulfur (GMC–S) film, with MC–sulfur spheres as "active islands" and graphene sheets as "trapping nets", exhibits good cycling stability (500 cycles, with a capacity retention of 85%) with a high specific capacity of 1322 mA h g^{-1} at 0.1C.

Lithium–sulfur (Li–S) batteries, with a theoretical capacity of 1675 mA h g^{-1} and a high power density up to 2600 W h kg^{-1}, are considered as a promising candidate to replace the state-of-the-art lithium ion batteries.[1] Specifically, a sulfur cathode can offer an order of magnitude higher capacity at an operating voltage of 2.1 V than the commercial cathode material, which will further contribute to the high energy density of Li–S batteries.[2] However, the practical application of Li–S batteries is severely restricted by several issues: (i) low utilization of a sulfur cathode as a result of the insulating nature of pure sulfur as well as its discharge products; (ii) poor cycling stability and serious self-discharge due to the inevitable dissolution of the polysulfide (Li_2S_n) intermediates into electrolyte and consecutively shuttling to the anode side.[3]

Several approaches have been proposed to address these problems. Particularly, various kinds of carbon matrices with good electrical conductivity[4] and porous structures[5] are considered as perfect guest species, in order to increase the utilization efficiency of the sulfur materials.[6] Carbon nanotubes (CNTs), graphene sheets, and nanostructured porous carbon materials are highly desired to fabricate carbon/sulfur (C/S) composites, in which mesoporous carbon (MC) spheres are considered as promising candidates to load active sulfur in their internal channels.[7] However, the "shuttling effect" of Li_2S_n, in fact, cannot be efficiently restricted by the mesoporous carbon matrix,[8] although a high content of sulfur is achieved. A "core–shell" morphology with sulfur as the "core" and net layers as the "shell" may provide great opportunities for developing hierarchical sulfur-based cathode materials.

In this work, a new graphene sheet–mesoporous carbon sphere–sulfur (GMC–S) film with interconnected micro/mesopores as well as highly electrical conductivity was successfully developed. A large amount of active sulfur was loaded in the channels of MC materials. Graphene sheets intercalated in the mesoporous carbon–sulfur (MC/S) hybrids can greatly enhance the electrical conductivity of the prepared GMC–S film, meanwhile act as a "shell" to restrict the "shuttling" of Li_2S_n. Based on this account, an excellent electrochemical performance of the GMC–S film, including high specific capacity (up to 1322 mA h g^{-1}) and long-term cycling properties (500 cycles with a capacity retention of 84%), has been achieved due to the synergistic effect of the hierarchical carbon matrix and the active sulfur material.

Flexible GMC–S films were fabricated by a facile method: vacuum filtration of graphene oxide (GO) sheets/MC–S hybrids and chemical reduction of GO/MC–S films with hydrazine vapor (Fig. 1a). A large amount of lithium ion (Li^+) can be inserted into or extracted from MC–S spheres (Fig. 1b). A uniform sphere morphology with a size of approximately 120 nm can be observed (Fig. S1, ESI†). Due to the ordered hexagonal arrays of MC sphere, N_2 adsorption/desorption analysis of MC spheres exhibits a high specific surface area of 987 m^2 g^{-1} with a total pore volume of 3.7 cm^3 g^{-1} (Fig. S2, ESI†). Fig. S3 (ESI†) exhibits the SEM images of MC–S hybrids (Fig. S3a, ESI†), coupling the energy dispersive spectroscopy (EDS) mapping images of carbon (C), silicon (Si) and sulfur (S) (Fig. S3b–S2d, ESI†). The homogeneous sulfur distribution confirms the successful loading of active sulfur. A high sulfur content up to 90% was detected by the EDS spectrum (Fig. S3e, ESI†). The dramatically decreased specific surface area (79 m^2 g^{-1}, Fig. S4, ESI†) of the MC–S hybrid resulted from the high content of sulfur. XRD patterns and TGA analysis of the prepared MC–S hybrids are presented (Fig. S5, ESI†). MC–S hybrids show apparent characteristic diffraction peaks of sulfur apart from the broad diffraction peak at $2\theta = 25^\circ$, which can be ascribed to the typical *F*ddd orthorhombic sulfur diffraction peaks,[9] as indicated by the blue curve of pure S (Fig. S5a, ESI†).

[a] *School of Chemistry and Chemical Engineering, Jiangsu Key Laboratory of Green Synthetic Chemistry for Functional Materials, Jiangsu Normal University, Xuzhou 221116, China. E-mail: yanyan@jsnu.edu.cn*

[b] *State Key Laboratory for Modification of Chemical Fibers and Polymer Materials, College of Materials Science and Engineering, Donghua University, Shanghai 201620, China. E-mail: txliu@dhu.edu.cn*

† Electronic supplementary information (ESI) available: SEM, TGA, TEM, XPS, and partial electrochemical performances. See DOI: 10.1039/c7cc04523a

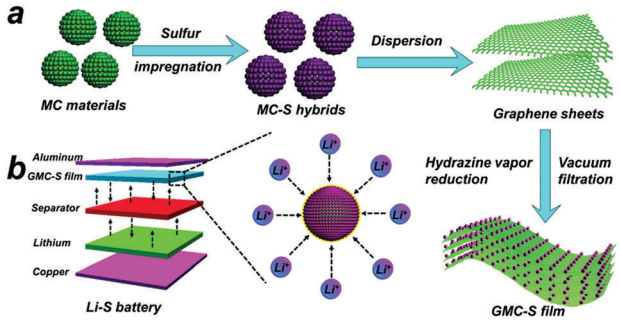

Fig. 1 (a) Fabrication of the GMC–S film and (b) rapid insertion/extraction of Li^+ on MC–S hybrids.

TGA analysis indicates that a high sulfur content of 88% has been achieved (Fig. S5b, ESI†), which is comparable to the result (90%) from the EDS spectrum.

A free-standing GMC–S film has been developed with MC–S hybrids inserted into the intervals of graphene layers (Fig. S6, ESI†). A cross section of the GMC–S film with a thickness of ~6 μm (Fig. 2a) confirms the homogeneous dispersion of MC–S hybrid spheres. Meanwhile, good porosity (Fig. 2b–d) was created between different crumpled graphene layers due to the insertion of MC–S hybrids. These macropores can provide a sufficient expansion space for the chemical lithiation of active sulfur. EDS mappings of the cross section of the GMC–S film (Fig. S7, ESI†) further confirm the good dispersion of MC–S spheres. Interestingly, the GMC–S film exhibits excellent flexibility (Fig. 2e), which allows it to be used as a working electrode directly in an integrated membrane without any binder additions. Furthermore, the prepared GMC–S film possesses a high electrical conductivity up to 105 S cm^{-1}, yet achieving a high sulfur loading of 65% (Fig. S8, ESI†). Three stably lighted

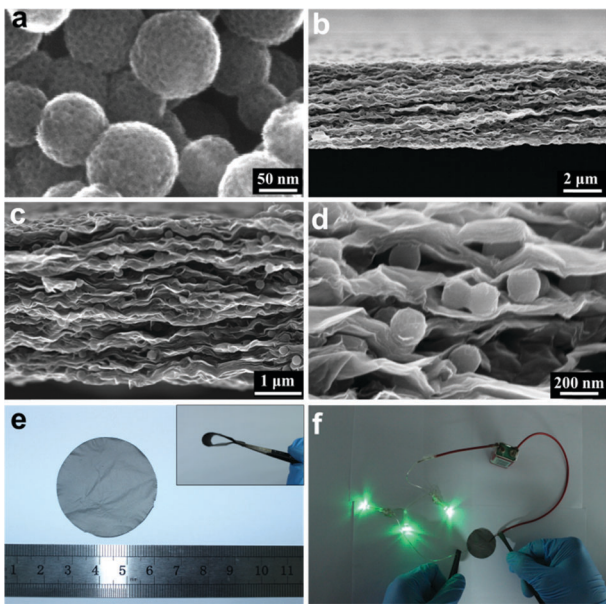

Fig. 2 SEM images of (a) MC spheres and (b–d) the GMC–S film with different magnifications. (e) Photograph of the GMC–S film with flat and curved structures. (f) Copper wire can be replaced by the GMC–S film in a conductive pathway.

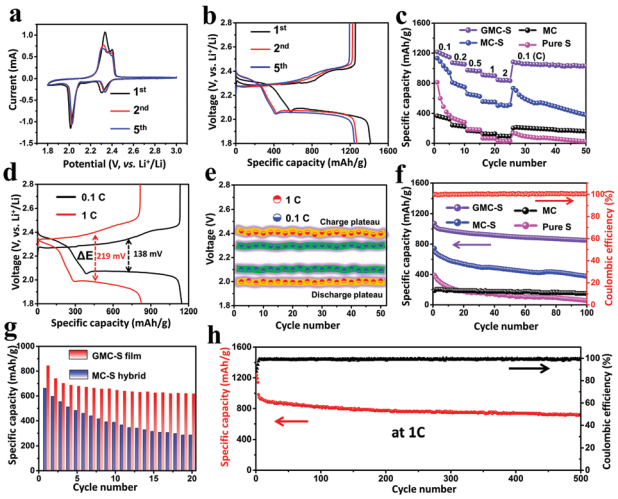

Fig. 3 Electrochemical performances of GMC–S films. (a) Charge/discharge curves at 0.1C and (b) CV curves at 0.1 mV s^{-1} on the 1st, 2nd and 5th cycles of the Li–S battery with the GMC–S electrode. (c) Rate capabilities of different materials of MCs, MC–S hybrids, GMC–S films and pure S from 0.1 to 2C. (d) Comparison of charge/discharge curves at 0.1 and 1C of the GMC–S electrode. (e) Voltage plateaus in charge/discharge processes over 50 cycles at 0.1 and 1C of the GMC–S electrode. (f) Discharge capacities of MCs, MC–S hybrids, GMC–S films and pure S over 100 cycles at 0.5C. (g) Discharge capacities of the GMC–S films and MC–S hybrids at low voltage plateau. (h) Long-term cycling stability of the GMC–S electrode over 500 times at 1C.

light-emitting diodes (LEDs) in a closed circuit further confirm that the GMC–S film can be directly used as an electrode material. High-resolution XPS spectra of C 1s region (Fig. S9, ESI†) with oxygen-containing groups overwhelmingly diminished, which further confirms the electrical conductivity of the GMC–S film.

Electrochemical performances of Li–S batteries compared with those of GMC–S electrodes, MC spheres, MC–S hybrids and pure S are illustrated in Fig. 3. CV curves of a Li–S battery with a GMC–S electrode exhibit two main reduction peaks at 2.34 and 2.01 V (Fig. 3a), corresponding to the transformation from cyclo-S_8 to high-order Li_2S_n and further sequential reduction to lithium sulfide (Li_2S_2 and Li_2S).[8a,10] In the anodic scan, two strong oxidation peaks at 2.36 and 2.39 V have been observed, indicating the coupled conversion from lithium sulfide to Li_2S_x and finally to an S_8 molecule.[11] No apparent shift of oxidation and reduction peaks was observed in the 2nd and 5th cycles, indicating that the polarization effect merely occurred in the GMC–S film. Two voltage plateaus at ~2.30 and ~2.03 V in the discharge curves of GMC–S were observed (Fig. 3b) due to the two-step quasi-dynamic-equilibrium reactions of sulfur and lithium.[3c,12] Also, a higher reversible specific capacity up to 1204 mA h g^{-1} at 0.1C was achieved, compared to the lower values of MC materials (298 mA h g^{-1}), MC–S hybrids (1022 mA h g^{-1}) and pure S (633 mA h g^{-1}) (Fig. S10, ESI†). The cycling stability of the GMC–S film can be further confirmed by the stable CV curves up to the 30th cycle (Fig. S11, ESI†). Besides, a reversible specific capacity of 1168 mA h g^{-1} can be achieved when the current density was recovered back to 0.1C (Fig. 3c). The XPS survey of the GMC–S film exhibits apparent S2s and S2p peaks (Fig. S12a, ESI†). In the S2p spectrum (Fig. S12b, ESI†), two peaks anchored at 163.9 eV ($S2p_{3/2}$) and 165.1 eV ($S2p_{1/2}$), coupling the peak at 168.4 eV (C–SO_x–C),

represent that the S atoms are connected to carbon atoms, resulting in the stable C–S bond formed between the active sulfur and the carbon matrix.

Contrarily, the CM–S hybrid undergoes a severe capacity decrease under the same testing rates (Fig. 3c), indicating severe polarization and distortion occurring in the MC–S electrode without the protection of graphene sheets. Charge/discharge curves of a GMC–S electrode exhibit flat and stable plateaus at 0.1C with a low polarization of 138 mV, which increases to 219 mV as the current density was enhanced to 1C (Fig. 3d). These results suggest a kinetically efficient reaction process of a GMC–S electrode with a very small barrier.[13] Capacity maintenance at a high rate and polarization under high current density were regarded as two characteristics to evaluate the rate performance of a Li–S battery.[3b] The voltage gap between the charge/discharge plateaus was slightly enlarged and stably kept up to 50 cycles when the current density was increased from 0.1 to 1C (Fig. 3e), which agrees well with the good rate capability of a GMC–S electrode (Fig. 3c). The Li–S battery with the GMC–S electrode shows a stable cycling performance (Fig. 3f) with a high specific capacity of 885 mA h g^{-1} maintained. Comparatively, severe capacity decrease occurred in the cycling performance of both MC–S hybrids and pure S electrodes. Furthermore, the capacity decay mechanism of the GMC–S electrode is also investigated. The discharge curve of the GMC–S film can be divided into high and low plateaus (Fig. S13, ESI†), where a lower voltage plateau represents the conversion from Li_2S_n to lithium sulfur and a higher voltage plateau can be specified to the back-formation of Li_2S_n. Fig. 3g exhibits the specific capacities calculated from the lower voltage plateaus of the GMC–S film and the MC–S hybrid. The severely decreased low voltage plateau capacity of the MC–S hybrid compared with the good cycling stability of the GMC–S film adequately suggests the perfect "net effect" of graphene layers for retarding the dissolution of Li_2S_n. Interestingly, the Li–S battery with the GMC–S film can also show a favorable long-term cycling stability over 500 cycles at 1C, coupling with a Coulombic efficiency of 99% (Fig. 3h). Also, the homogeneously dispersed sulfur element in the cycled GMC–S film (Fig. S14, ESI†) confirms the effective "shuttling" restriction effect of the crumpled graphene sheets.

Electrochemical impedance spectroscopies (EIS) of Li–S batteries at different cut-off voltages (Fig. S15a, ESI†) have been recorded in order to elucidate the resistance dependency, as seen in Fig. S15b (ESI†). Each Nyquist plot exhibits a medium-to-high frequency semicircle, as well as a long inclined line in the low frequency region that corresponds to the Warburg impedance. An intercept on the real axis in the high frequency is the ohmic resistance (R_e) that includes the electrolyte and electrode resistances. Meanwhile, the interfacial charge-transfer (R_{ct}) resistance of the battery can be calculated from the semicircle in the medium-to-high frequency.[14] The R_e and T_{ct} values calculated according to the established equivalent circuit (Fig. S16, ESI†) are depicted in Fig. S15c (ESI†). It can be observed that the R_{ct} values were sensitively changed in accordance with the transition from an S_8 molecule, Li_2S_n, to an insulated lithium sulfide, while the R_e was not. Furthermore, a newly emerged resistance (R_s) resulting from the solid-electrolyte-interface (SEI) film can be detected according to the semicircle in the medium-frequency region of the Nyquist files with the increase of cycle times (Fig. S15d, ESI†). The fitted values of R_e, R_s, and R_{ct} have been compared and are listed in Fig. S15e (ESI†). The R_e and R_{ct} values were slightly varied due to the contribution of the activation effect on the first cycle. However, the SEI resistance gradually emerged and increased, which reasonably results in the stepwise decrease of the specific capacities of the Li–S battery (Fig. S17, ESI†). In other words, the capacity decrease resulted from the "diffusing" effect of Li_2S_n can be efficiently prevented due to the effective protection from graphene sheets.

Fig. S18 (ESI†) shows the SEM images of the GMC–S films with different MC–S spheres. The sulfur contents of these films were about 45%, 55%, 67% and 74% (Fig. S19, ESI†). Here, these GMC–S films were denoted as GMC–S4, GMC–S5, GMC–S6 and GMC–S7. The film morphology (Fig. S18a, d, g and j, ESI†) of these GMC–S materials can be obtained with porous structures (Fig. S18c, f, i and l, ESI†). Also, MC–S hybrid spheres can be homogeneously dispersed throughout the GMC–S film, which can be further confirmed by the TEM image of GMC–S7 (Fig. S20, ESI†).

Electrochemical charge/discharge curves of GMC–S4, GMC–S5, GMC–S6 and GMC–S7 are listed in Fig. 4a. Based on the calculations of the weight of the GMC–S electrode, the specific capacities of these GMC–S4, GMC–S5, GMC–S6 and GMC–S7 films are about 833, 1012, 1245, and 1322 mA h g^{-1}, respectively. The specific capacities of these GMC–S films are compared in Fig. 4b. A purple LED can be easily lighted up in a closed circuit powered by the Li–S battery with a GMC–S7 electrode (Fig. 4c). In addition, the GMC–S7 film shows a good rate performance from 0.1 to 2.0C, and exhibits a high specific capacity of 1244 mA h g^{-1} when the current density was back to 0.1C (Fig. S21, ESI†). The long-term cycling performance of the GMC–S7 electrode was investigated (Fig. 4d), which delivers a stable capacity of 800 mA h g^{-1} after 500 cycles at 1C with a high Coulombic efficiency of 99%. Here, the GMC–S8 film with a higher sulfur content of 80% (Fig. S22 and S23, ESI†) was also investigated. However, the film morphology of the GMC–S8 material cannot be maintained due to the drawback of a connection between different graphene sheets, resulting in scattered fragments (Fig. S24, ESI†).

The GMC–S7 film exhibits more balanced performance compared with other reported carbon–sulfur composite electrodes including SPMC700,[15] GSH@APC,[8a] S/MMCS,[7a] and so on (Fig. S22a, ESI†). The remarkably improved electrochemical performance for these GMC–S films, such as high specific capacities and long-term cycling stabilities, can be ascribed to the synergistic effect between the MC–S hybrid and graphene sheets in the following four aspects. Firstly, a large amount of active sulfur can be loaded by the MC materials with an ultrahigh specific surface area. Secondly, the effective electrical conductive pathway can be established with graphene sheets inserting into MC–S hybrids, resulting in an excellent electron transfer ability of the obtained GMC–S films. Thirdly, Li_2S_n can be adsorbed by the crumpled graphene sheets, and their "shuttling effect" can be further efficiently restricted according to the "net" effect of graphene (Fig. S22b, ESI†), thus contributing to an improved capacity retention. Last but not the least, with flexible graphene sheets acting as a buffer layer, the GMC–S films will not suffer large stress by providing a sufficient space for the expansion of Li_2S_n during the lithiation/delithiation process, which benefits the good electrical contact between active sulfur and the conductive matrix, meanwhile contributing to the ultra-long cycling life of the GMC–S films.

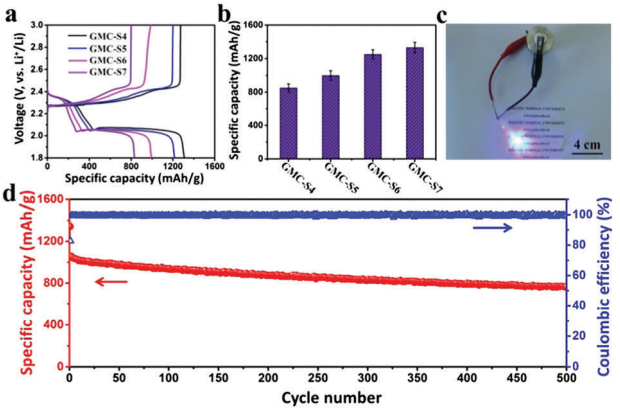

Fig. 4 Electrochemical performance of Li–S batteries with different GMC–S electrodes. (a) Charge/discharge curves at 0.1 C and (b) specific capacities of Li–S batteries with GMC–S4, GMC–S5, GMC–S6 and GMC–S7 electrodes. (c) A purple LED can be lit up by a Li–S battery with the GMC–S7 electrode. (d) Long-term cycling performance of a Li–S battery with the GMC–S7 electrode.

In summary, a high-performance carbon–sulfur cathode of GMC–S has been synthesized *via* confining sulfur within highly ordered MC spheres and further being wrapped by flexible graphene sheets. MC materials with high pore volume and highly ordered channels have loaded a large amount of sulfur. MC–S spheres acting as "islands" inside the GMC–S film ensure a sufficient insertion/extraction of Li^+. Crumpled graphene sheets with high flexibility provide excellent porous structures, which affords a sufficient space for the lithiation expansion of sulfur, meanwhile greatly improving the electrical conductivity of the GMC–S film. Furthermore, graphene sheets acting as porous "nets" can wrap the active MC–S hybrids to restrict the "shuttle" diffusion of Li_2S_n. The free-standing GMC–S film culminates in a decent electrochemical performance including an ultrahigh specific capacity (1322 mA h g^{-1}) and a long-term cycling stability (500 cycles with capacity retention of 85%) with a high Columbic efficiency up to 99%. These results demonstrate that the GMC–S film is a promising cathodic candidate for Li–S batteries in practical applications. Meanwhile, this synthetic strategy can provide a general but effective approach to develop integrated electrodes without binder additions for energy storage devices including sodium/lithium ion batteries, supercapacitors, and so on.

This work was supported by the National Natural Science Foundation of China (No. 51125011 and 51433001), the Natural Science Foundation of Jiangsu Province (BK20150238), and the Project Funded by the Priority Academic Program Development of Jiangsu Higher Education Institutions.

Notes and references

1 (*a*) A. Manthiram, S. H. Chung and C. Zu, *Adv. Mater.*, 2015, **27**, 1980; (*b*) J. Schuster, G. He, B. Mandlmeier, T. Yim, K. T. Lee, T. Bein and L. F. Nazar, *Angew. Chem., Int. Ed.*, 2012, **51**, 3591; (*c*) J. L. Shi, C. Tang, H. J. Peng, L. Zhu, X. B. Cheng, J. Q. Huang, W. Zhu and Q. Zhang, *Small*, 2015, **11**, 5243; (*d*) H. Wang, W. Zhang, H. Liu and Z. Guo, *Angew. Chem., Int. Ed.*, 2016, **55**, 3992; (*e*) Z. Li, J. Zhang, B. Guan, D. Wang, L. Liu and X. W. D. Lou, *Nat. Commun.*, 2016, **7**, 13065; (*f*) H. Wang, C. Zhang, Z. Chen, H. K. Liu and Z. Guo, *Carbon*, 2015, **81**, 782.

2 (*a*) J. Song, M. L. Gordin, T. Xu, S. Chen, Z. Yu, H. Sohn, J. Lu, Y. Ren, Y. Duan and D. Wang, *Angew. Chem., Int. Ed.*, 2015, **54**, 4325; (*b*) L. Sun, D. Wang, Y. Luo, K. Wang, W. Kong, Y. Wu, L. Zhang, K. Jiang, Q. Li, Y. Zhang, J. Wang and S. Fan, *ACS Nano*, 2016, **10**, 1300; (*c*) F. Nitze, K. Fossum, S. Xiong, A. Matic and A. E. C. Palmqvist, *J. Power Sources*, 2016, **317**, 112.

3 (*a*) Z. Sun, S. Wang, L. Yan, M. Xiao, D. Han and Y. Meng, *J. Power Sources*, 2016, **324**, 547; (*b*) X. Fang, W. Weng, J. Ren and H. Peng, *Adv. Mater.*, 2016, **28**, 491; (*c*) Q. Sun, X. Fang, W. Weng, J. Deng, P. Chen, J. Ren, G. Guan, M. Wang and H. Peng, *Angew. Chem., Int. Ed.*, 2015, **54**, 10539; (*d*) H. Peng, W. Xu, L. Zhu, D. Wang, J. Huang, X. Cheng, Z. Yuan, F. Wei and Q. Zhang, *Adv. Funct. Mater.*, 2016, **26**, 6351.

4 (*a*) Z. Yang, H. Sun, T. Chen, L. Qiu, Y. Luo and H. Peng, *Angew. Chem., Int. Ed.*, 2013, **125**, 7693; (*b*) J. Huang, H. Peng, X. Liu, J. Nie, X. Cheng, Q. Zhang and F. Wei, *J. Mater. Chem. A*, 2014, **2**, 10869.

5 (*a*) Y. Fang, D. Gu, Y. Zou, Z. Wu, F. Li, R. Che, Y. Deng, B. Tu and D. Zhao, *Angew. Chem., Int. Ed.*, 2010, **49**, 7987; (*b*) W. Li, F. Wang, Y. Liu, J. Wang, J. Yang, L. Zhang, A. A. Elzatahry, D. Al-Dahyan, Y. Xia and D. Zhao, *Nano Lett.*, 2015, **15**, 2186; (*c*) G. Zhou, L. Li, C. Ma, S. Wang, Y. Shi, N. Koratkar, W. Ren, F. Li and H. Cheng, *Nano Energy*, 2015, **11**, 356; (*d*) L. Zhu, H. Peng, J. Liang, J. Huang, C. Chen, X. Guo, W. Zhu, P. Li and Q. Zhang, *Nano Energy*, 2015, **11**, 746; (*e*) Y. Chen, S. Lu, X. Wu and J. Liu, *J. Phys. Chem. C*, 2015, **119**, 10288.

6 S. Zhu, Y. Wang, J. Jiang, X. Yan, D. Sun, Y. Jin, C. Nan, H. Munakata and K. Kanamura, *ACS Appl. Mater. Interfaces*, 2016, **8**, 17253.

7 (*a*) Z. Li, Y. Jiang, L. Yuan, Z. Yi, C. Wu, Y. Liu, P. Strasser and Y. Huang, *ACS Nano*, 2014, **8**, 9295; (*b*) T. Xu, J. Song, M. L. Gordin, H. Sohn, Z. Yu, S. Chen and D. Wang, *ACS Appl. Mater. Interfaces*, 2013, **5**, 11355; (*c*) G. He, S. Evers, X. Liang, M. Cuisinier, A. Garsuch and L. F. Nazar, *ACS Nano*, 2013, **7**, 10920; (*d*) Z. Guo, D. Zhou, H. Liu, X. Dong, S. Yuan, A. Yu, Y. Wang and Y. Xia, *J. Power Sources*, 2015, **276**, 181; (*e*) Y. Fang, Y. Lv, R. Che, H. Wu, X. Zhang, D. Gu, G. Zheng and D. Zhao, *J. Am. Chem. Soc.*, 2013, **135**, 1524.

8 (*a*) H.-J. Peng, J.-Q. Huang, M.-Q. Zhao, Q. Zhang, X.-B. Cheng, X.-Y. Liu, W.-Z. Qian and F. Wei, *Adv. Funct. Mater.*, 2014, **24**, 2772; (*b*) J. G. Werner, S. S. Johnson, V. Vijay and U. Wiesner, *Chem. Mater.*, 2015, **27**, 3349; (*c*) M.-S. Park, B. O. Jeong, T. J. Kim, S. Kim, K. J. Kim, J.-S. Yu, Y. Jung and Y.-J. Kim, *Carbon*, 2014, **68**, 265.

9 (*a*) Z. Lyu, D. Xu, L. Yang, R. Che, R. Feng, J. Zhao, Y. Li, Q. Wu, X. Wang and Z. Hu, *Nano Energy*, 2015, **12**, 657; (*b*) K. Mi, Y. Jiang, J. Feng, Y. Qian and S. Xiong, *Adv. Funct. Mater.*, 2016, **26**, 1571; (*c*) M. Oschatz, J. T. Lee, H. Kim, W. Nickel, L. Borchardt, W. I. Cho, C. Ziegler, S. Kaskel and G. Yushin, *J. Mater. Chem. A*, 2014, **2**, 17649.

10 (*a*) G. He, B. Mandlmeier, J. Schuster, L. F. Nazar and T. Bein, *Chem. Mater.*, 2014, **26**, 3879; (*b*) F. Sun, J. Wang, H. Chen, W. Li, W. Qiao, D. Long and L. Ling, *ACS Appl. Mater. Interfaces*, 2013, **5**, 5630.

11 (*a*) Q. Sun, B. He, X.-Q. Zhang and A.-H. Lu, *ACS Nano*, 2015, **9**, 8504; (*b*) J. Balach, H. K. Singh, S. Gomoll, T. Jaumann, M. Klose, S. Oswald, M. Richter, J. Eckert and L. Giebeler, *ACS Appl. Mater. Interfaces*, 2016, **8**, 14586.

12 H. Hu, H. Cheng, Z. Liu, G. Li, Q. Zhu and Y. Yu, *Nano Lett.*, 2015, **15**, 5116.

13 (*a*) G. Zhou, S. Pei, L. Li, D. W. Wang, S. Wang, K. Huang, L. C. Yin, F. Li and H. M. Cheng, *Adv. Mater.*, 2014, **26**, 625; (*b*) J. Balach, T. Jaumann, M. Klose, S. Oswald, J. Eckert and L. Giebeler, *Adv. Funct. Mater.*, 2015, **25**, 5285.

14 J. Song, T. Xu, M. L. Gordin, P. Zhu, D. Lv, Y.-B. Jiang, Y. Chen, Y. Duan and D. Wang, *Adv. Funct. Mater.*, 2014, **24**, 1243.

15 X. Zhao, Y. Liu, J. Manuel, G. S. Chauhan, H. J. Ahn, K. W. Kim, K. K. Cho and J. H. Ahn, *ChemSusChem*, 2015, **8**, 3234.

